http://dx.doi.org/10.4322/polimeros.2013.079

The Influence of Screw Configurations and Feed Mode on the Dispersion of Organoclay on PP

Kelly S. Santos, Renan Demori, Raquel S. Mauler
Instituto de Química, Universidade Federal do Rio Grande do Sul, UFRGS

Susana A. Liberman; Mauro A. S. Oviedo
Braskem S/A, III Pólo Petroquímico

Abstract: The design of the screw configuration as well as the screw speed, the residence time, the feeder type, and the temperature has a large effect on the dispersion of the clay into the matrix and, consequently, on the mechanical and thermal properties of the polymeric matrix. The objective of the present work was to evaluate the influence of two different screw configurations (left-handed elements) and the feed type (hopper or side feeder) on the dispersion of 5 wt% Cloisite 20A into the PP matrix without the use of compatibilising agents. In profile 1 (lower shear), the 5 wt% C20A/PP (PPC20AP1) nanocomposite morphology presented elliptical agglomerated structures with compacted platelets, whereas in the profile 2, the 5 wt% C20A/PP (PPC20AP2) showed elongated forms with better separated platelets and a better clay distribution into the PP matrix. When the side feeder mode was used in profile 2, a mix of elliptical and elongated structures with some individual clay sheets was observed.The neat PP showed the same tensile modulus and impact strength in both screw configurations. The PPC20AP1 presented a tensile modulus and an impact strength that was lower than the PPC20AP2, because in profile 2 the pressure and residence time are higher due to the two left-handed elements. Thus, the dispersion and distribution of the clay throughout the matrix were improved, and the agglomerated structures were reduced. When the side feeder mode was used, there was a decrease in the PP/clay mechanical properties, but the values found were higher than those in profile 1.

Keywords: *PP nanocomposites, processing conditions, properties, morphology.*

Introduction

Polypropylene/montmorillonite (PP/MMT) is one of the most commonly studied nanocomposites to improve several properties. PP/MMTs are produced using many technologies, and their applications include a range of manufacturing processes at a relatively low cost[1,2]. There is much evidence that supports melting processing as the preferred production method of PP/MMT for commercial use[3-7]. Additionally, the literature suggests that the exfoliation and the dispersion of nanoclays in polypropylene requires the exchange of the sodium cations that are present in the nanoclay layers with the organophilic cations (dimethyl, dihydrogenated tallow, and quaternary ammonium chloride), which alters the initial interlayer spacing and improves the interaction between the clay and the PP[8,9].

Predicting whether a polymer and organoclay (OMMT) will form a true nanocomposite through melt compounding is not easy because there are many factors influencing the outcome[10]. The improvements in the final properties usually depend on the degree of exfoliation, delamination, and dispersion of the clay into the matrix[11-13]. Fine control of the interfacial morphology of polymer nanocomposites is critical to imparting the desired mechanical properties to such materials[14-16].

Within the nanocomposite literature, the effects of clay modification[17], the clay content and the use of different compatibiliser agents to increase the compatibility of the clay and the polymer[18,19] have all been studied extensively. However, the importance of the processing conditions has not been adequately explored because of the complex interactions between the experimental factors and the structural control in these types of systems. Furthermore, optimising the processing parameters is key to maximising the interfacial contact between the polymer and the clay and to enhancing the macroscopic properties of the resulting nanocomposites[20,21]. Previous studies have suggested that it is important to use processing equipment that is flexible in design with the capability to control the residence time with dispersive and distributive mixing. Both the feed location and the order of feeding are also important considerations when designing the compounding process[4,11].

The screw configuration, the screw speed, the residence time, the feeder type, and the temperature of the melt process all have a large effect on the dispersion of the clay in the polymer matrix[22]. Therefore, the screw profile design plays a key role in controlling the morphology of the nanocomposite[11].

Based on the literature, changes in the processing conditions and the screw profiles greatly affect the properties of the nanocomposites because the clay sheets can break during the shear processing, which decreases the final aspect ratio of these materials[23,24]. Some researchers have produced polar polymer/OMMT nanocomposites with intercalated and exfoliated morphologies using a co-rotating twin or single screw extruder. They have found that optimising the shear intensity and the residence time in the extruder generally improved the delamination and the dispersion of the MMT in the polymer matrix[4,11,25,26].

However, when using incompatible organoclay and apolar polymers, the optimisation of the processing conditions is even more important for achieving smaller agglomerated structures and partial exfoliation as well as preserving the aspect ratio of the clay platelets in the matrix[27]. To achieve good dispersion of the clay, it is important to understand how the processing conditions affect the morphology of PP/MMT nanocomposites and their final properties[14,28].

The aim of this work was to study the influence of two different screw configurations, each with a different shear rate, and two different feed types (i.e., hopper or side feeder) on the morphological, thermal, and mechanical properties of PP/MMT nanocomposites. The melting process was used without a compatibilising agent to isolate and to better evaluate the effect

***Corresponding author: Raquel S. Mauler**, Instituto de Química, Universidade Federal do Rio Grande do Sul – UFRGS, Av. Bento Gonçalves, 9500, CEP 91501-970, Porto Alegre, RS, Brazil, e-mail: raquel.mauler@ufrgs.br*

of processing conditions on the dispersion of the organoclay into the PP matrix.

Experimental

Materials

The polymer used was a commercial grade polypropylene homopolymer with a melt flow index (MFI) of 3.5 g/10 min (230 °C/ 2.16 kg) from Braskem S.A., Brazil.

The clay used was a commercial organoclay montmorillonite (OMMT) Cloisite 20A (C20A) that was modified with a quaternary ammonium salt and possessed a cation exchange capacity (CEC) of 95 meq/100 g from Southern Clay Products.

Nanocomposites preparation

The mixture was prepared using melt intercalation in a counter-rotating twin-screw extruder (Coperion ZSK18K38, screw diameter of 18 L/D = 44) operating at 350 rpm with a constant feed ratio of 3 kg/h and a temperature profile of 165, 170, 175, 175, 180, 185, 190 °C with 5 wt% of C20A. The PP nanocomposites were prepared with two different screw profile configurations that created a moderate shear rate (profile 1) and a high shear rate (profile 2) as shown in Figure 1. When studying profile 2, two forms of feeding were used. In the first form, the polymer and the organoclay were fed simultaneously into the main hopper at the beginning of the extruder. In the second, the organoclay was added separately from a side feeder after the fusion of the PP in the beginning of the extruder. Figure 1 and Tables 1 and 2 show the main difference between profiles 1 and 2; specifically, the use of one set of 45° kneading blocks followed by two left-handed elements that increased the resulting shear force and the residence time is shown. This change in the screw profile greatly influenced the quality of the dispersion and exfoliation of the clay and its distribution into the polymer matrix, resulting in the breakage of clay tactoids and the homogenous distribution of the clay particles into the melt matrix.

Characterisation

The residence times of the two different screw configuration profiles were measured using coloured pellets that were fed into the main hopper at the beginning of the extruder and timed until their arrival at the extruder die. Five measurements were performed for each screw configuration profile.

Samples for mechanical testing were prepared in a Battenfeld injection mould according to ASTM D 4101. Tensile testing was performed according to ASTM D638, specimen type 1 and was conducted on a universal tensile machine (EMIC DL 10000) at a speed of 50 mm/min. The Young modulus measurements were performed with extensometer. Izod Impact tests were performed at 23 °C using a pendulum-type impact tester (Ceast, Resilimpact) according to ASTM D 256.

A TA model QA 800 instrument was used for dynamic mechanical analyses (DMA) of the materials at a fixed frequency of 1 Hz. DMA analyses were performed in single cantilever mode, using specimens with approximate dimensions of 17.80 × 3.2 × 12.75 mm.

Thermal properties were determined using a DSC Thermal Analyst 2100 from TA Instruments. All measurements were performed under a nitrogen atmosphere. The samples were heated to between 50 and 200 °C at a heating and cooling rate of 10 °C/min. Melting temperature measurements were performed in the second

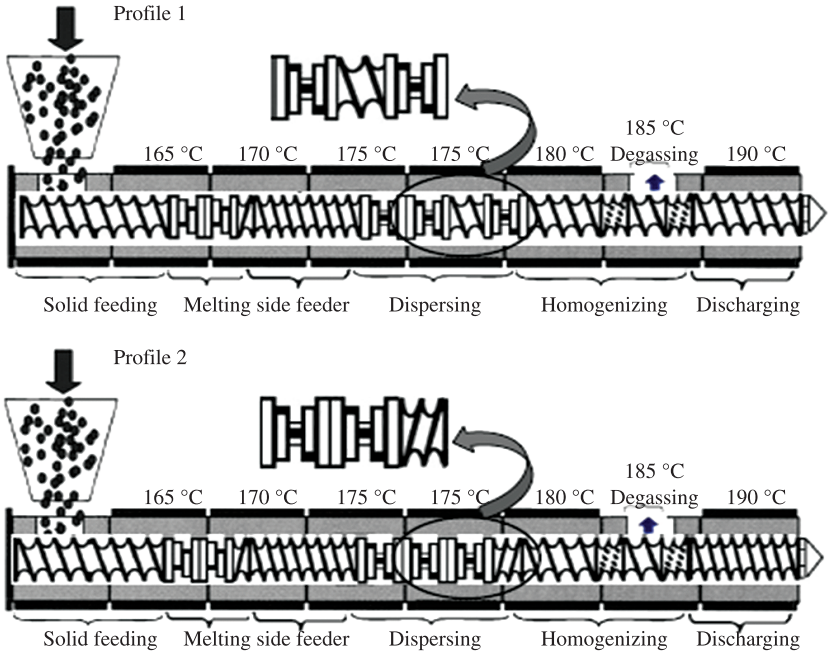

Figure 1. Scheme of the screw configuration design: Profile 1 (above) and Profile 2 (below).

Table 1. Screw configuration profile used to prepare the PP/5%C20A nanocomposites.

Screw Profile	Screw Configurations
Profile 1	T2–18–72 + T2–12–24 + K4–3–80–30° + T2–8–8L + T2–12–36 + T2–12–54 + T2–12–12 + K5–2–72–45° + T2–12–24 + K5–2–48–45° + T2–12–72 + D1–11–24L + T2–12–24 + D1–11–24L + T2–12–96 + T2–8–32
Profile 2	T2–18–72 + T2–12–24 + K4–3–80–30° + T2–8–8L + T2–12–36 + T2–12–54 + T2–12–12 + K5–2–120–45° + L2–8–16 + D1–11–24 + T2–12–24 + T1–11–24 + T2–12–96 + T2–8–16

T represents convey elements; K represents kneading block; L represents a reversed conveying screw elements; D represents dispersing elements.

heating cycle. The degree of crystallinity was determined using ΔH_m^0 =190 J/g for PP[29]. The DSC instrument was calibrated with indium before use. The thermal stability was measured using a thermo gravimetric analyser (TA model QA50). The samples (5-10.0 mg in film form) were heated from 30 to 900 °C at the rate of 20 °C/min under an inert nitrogen atmosphere (50 mL/min).

The transmission electron microscopy (TEM) images were obtained at 80 kV with a JEOL JEM-1200 Ex II. Ultrathin sections (70 nm thickness) of the specimens, which were cooled to –80 °C, were obtained using cryoultramicrotomy with a diamond knife that was also cooled to –80 °C. The sections were placed on 300 mesh Cu grids. The fracture surface of notched Izod impact specimens (cross-section) at room temperature was studied using field emission SEM (JEOL JSM-6060) after coating with carbon to minimise electrostatic charging. The fracture surface morphologies of neat PP and PP-clay nanocomposites were observed using an electron accelerating voltage of 10 kV.

Results and Discussion

Morphology of the PP/C-20A nanocomposites

The clay dispersion in the polymer matrix is directly related to the processing conditions[30]. The screw configuration can modify the original clay morphology because of the high shear forces that occur during processing[31]. Thus, the effect of processing conditions on the morphology of PP nanocomposites was studied using TEM to evaluate the magnitude of C20A intercalation or exfoliation into the matrix. TEM micrographs of PP/C20A nanocomposites (Figure 2) prepared using different shear rates showed an oriented

Table 2. Materials and processing conditions of the PP/5%C20A nanocomposites.

Samples	PP (%)	C-20A (%)	Profile	Residence time at 3.0 Kg/h (s)
PP P1	100	0	P1	33 ± 2
PP P2	100	0	P2	52 ± 1
PP C20A P1	95	5	P1	33 ± 2
PP C20A P2	95	5	P2	52 ± 1
PP C20A P2SF	95	5 (side feeder)	P2	52 ± 1

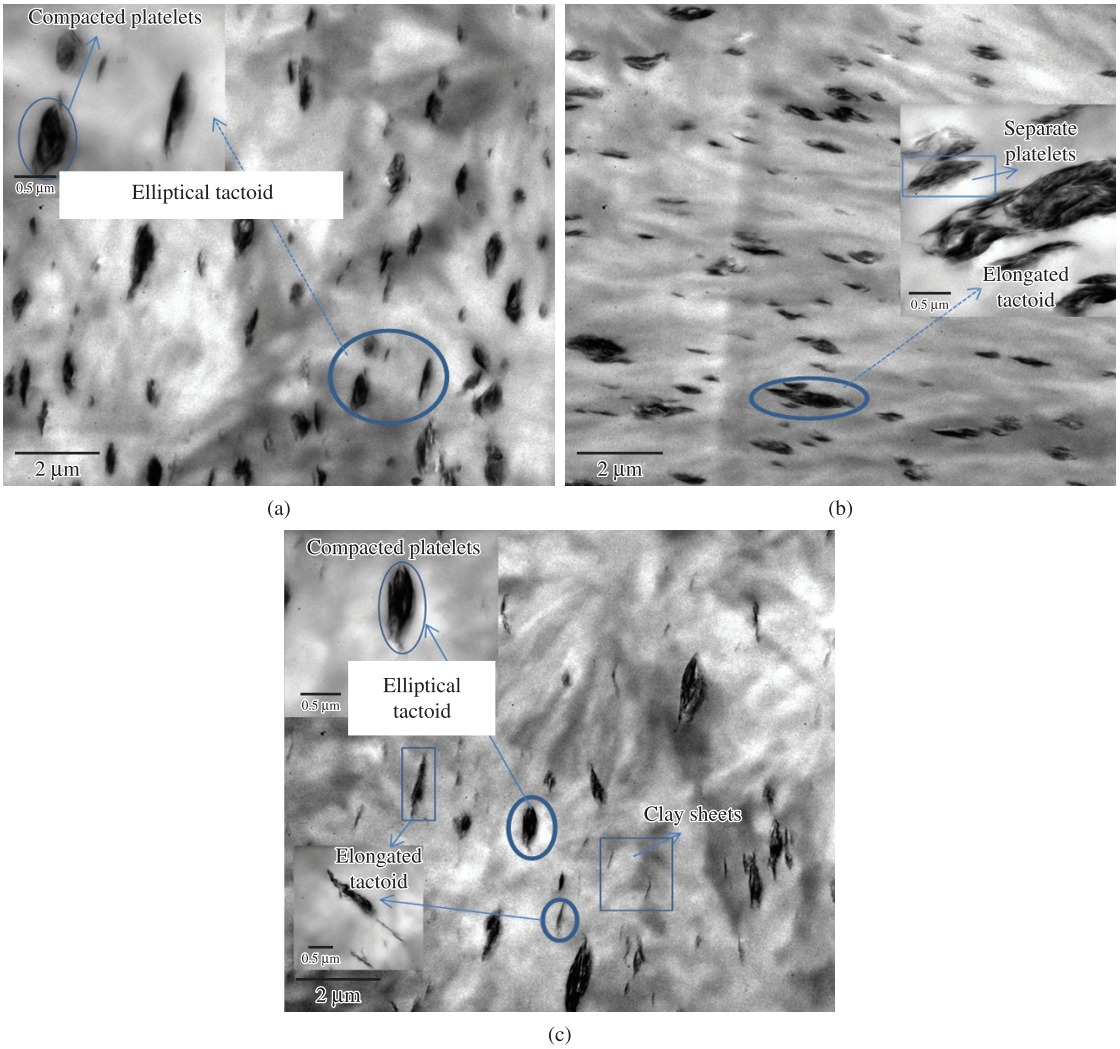

Figure 2. TEM micrographs of the PP-C20A nanocomposites prepared in the screw using Profile 1 (a), Profile 2 (b) and Profile 2 with side feeder (c).

dispersion of the nanofiller in the polymeric matrix. Agglomerates of different sizes and partially exfoliated structures were observed in all of the profiles. The PPC20AP1, prepared using the P1 profile (lower shear), presented elliptical agglomerated structures and more compacted platelets, whereas the PPC20AP2, prepared using the P2 profile (higher shear), presented elongated forms with better separated platelets more separated and a better clay distribution into the PP matrix. The increased shear in the P2 profile, promoted by the addition of two left hand elements after the single set of kneading block, facilitated the sliding of silicate sheets and increased the separation between the platelets, promoting a morphological change in the agglomerated structures of the C20A clay. Furthermore, this profile did not decrease the length of the platelets, but by reducing their thickness, the aspect ratio of the PPC20AP2 increased. When the side feeder mode (SF) was used in the P2 profile, the sample PPC20AP2SF showed a mix of elliptical and elongated structures with some individual clay sheets but with a poor distribution of the clay platelets. With this type of feeding, the nanoclay is added after the first set of kneading blocks and one left-handed element, which decreases the breaking efficiency and the separation of agglomerated structures.

Relationship among fractography, morphology and mechanical properties

The micrography of the impact fracture surfaces of the pristine PPP1 and PPP2 as well as the PP nanocomposites that were prepared using different shear profiles and feed types helped to better understand the effect of these processing conditions on the impact strength of these materials. This property is influenced by the form of the particles, the morphology, and the degree of interfacial adhesion between the clay and the matrix. In clay-reinforced semi-crystalline thermoplastic nanocomposites, the microdeformation processes identified as energy dissipating mechanisms, include crazing, cavitation or debonding of the clay particles with consequent microvoid formation with or without fibrillation, take to the posterior shear yielding of the matrix[32,33]. The great flexibility of the clay platelets allows them to bend and facilitates plastic deformation through the formation of microvoids between the layers[34]. The formation of microvoids occurs by the cavitation or debonding of the clay particles through the breaking, the opening or the sliding of the platelets[35]. Thus, increasing the number of microvoids with an elongated structure will increase the energy absorption by the shear yielding process. SEM micrographs of the pristine PPP1 and PPP2 as well as the PP nanocomposites that were prepared using different shear profiles and feed types clearly support this hypothesis. In Figure 3, the crack-propagation direction is indicated with a white arrow in the micrographs. The whole crack-propagation profiles of the materials are not shown because the mechanisms of energy dissipation were only observable in SEM images at higher magnification, so the close-up views of these profiles are shown in Figure 3. The fractured surface of the pristine PPP1 (Figure 3a) presented predominantly craze-like features without microvoid formation, whereas the PPP2 surface (Figure 3b) displayed a fibril network, which increased the effectiveness of the energy dissipation mechanisms. The samples with 5 wt% PPC20AP2 showed debonding of the clay particles with a smaller size than those of the PPC20AP1 samples (Figure 3c, d).

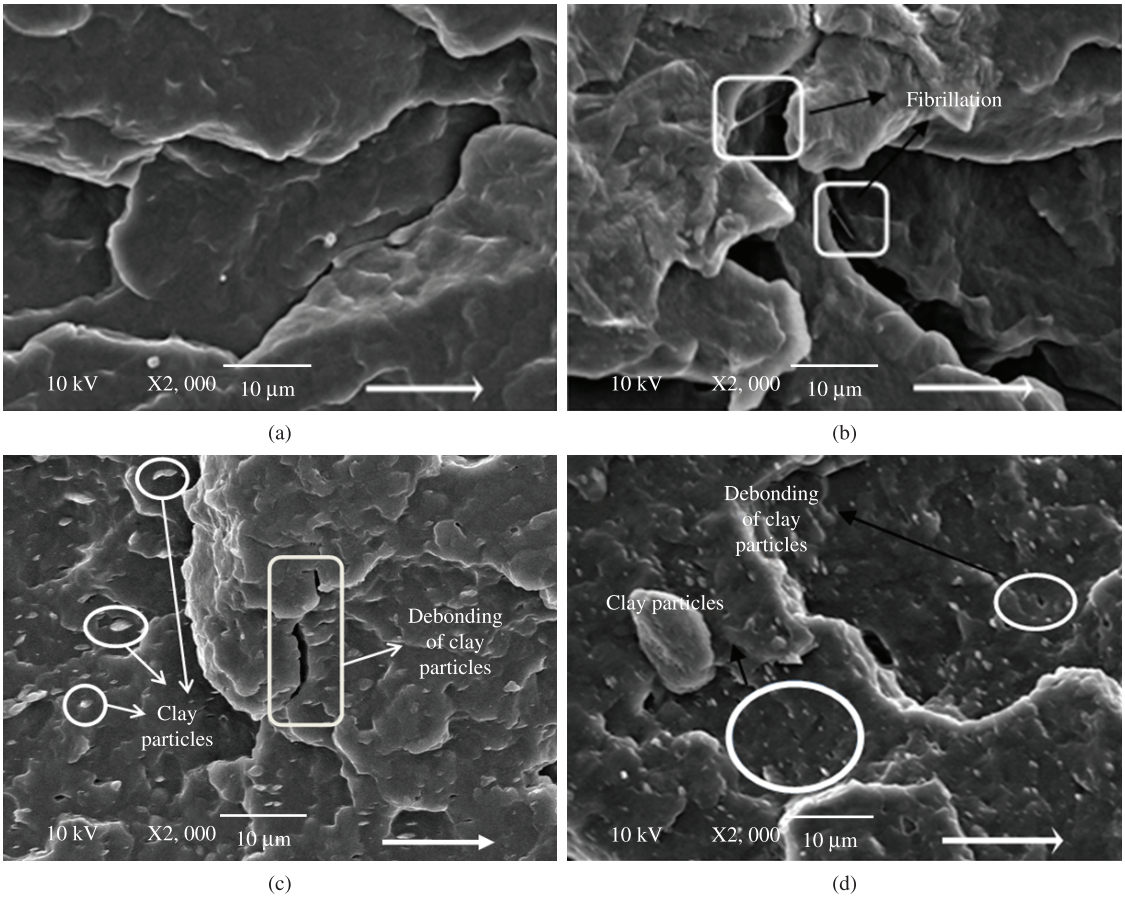

Figure 3. SEM images of PPP1 (a), PPP2 (b) and of PP/5%C20A nanocomposites prepared in profile 1 (c) and profile 2 (d).

As shown in Table 3, there were no significant changes in the impact strength or the modulus for the neat PP obtained by the different profiles. This finding shows that there were no significant breaks in the PP matrix chains obtained from the higher shear profile. However, profile 2 promoted significant changes in the distribution and the dispersion of the clay particles into the PP matrix, resulting in superior mechanical properties.

The addition of 5 wt% C-20A led to an increase in both the Young's modulus and the impact strength. The PPC20AP2 demonstrated a higher Young's modulus than the PPC20AP1 because of the existence of oriented and elongated structures, which improved the tensile strength of PP nanocomposite. Both the PPC20AP1 and the PPC20AP2 exhibited higher impact strengths than the corresponding neat PPP1 and PPP2; this increase was 16% and 44%, respectively. However, the PPC20AP2 exhibited a higher impact strength than the PPC20AP1. The elliptical structures in the PPC20AP1 probably acted as tension concentrators by reducing the impact strength compared to PPC20AP2, i.e., these elliptical structures acted as a conventional filler[36]. The Young's modulus value of the PPC20AP2SF was lower (10%) than the PPC20AP2 but was higher (11%) than the PPC20AP1 because the PPC20AP2SF contained a mix of elliptical and elongated structures. In addition, the impact strength was smaller in the PPC20AP2SF because there were fewer elongated structures with more platelets that were separated, which provided a larger contact surface between the PP and the clay and, consequently, the predominant energy dissipating mechanism was debonding of the clay platelets. The yield strain of PP/C20A samples was increased from 15% to 18% while the yield strength was maintained (Table 3).

The higher storage modulus of the PP nanocomposites for the entire temperature range studied indicated that the clay incorporation into the PP matrix promoted a positive reinforcement effect (Figure 4). Additionally, the storage modulus of the neat PP and the C20A nanocomposites at 23 °C followed similar trends in the Young's modulus although the variations were more significant (Table 3 and Figure 4a).

The β and α transitions in the tan δ curve provide an indication of the interactions between the matrix and filler. The region of the interphase surrounding the filler may change the physical properties of the nanocomposite. It has been reported that significant filler-matrix interactions decreased the β transition peak intensity because of reduced friction at the matrix-filler interface. However, the intensity of the β transition peak of the PP nanocomposites was similar to that of the neat polymers because of the absence of any compatibilising agent that could change the interface between the polymer and the organoclay (Figure 4b)[14].

The α transition peak, approximately at 73 °C, is related to relaxations of the intracrystalline amorphous chains of the PP, and its intensity is related to the amount of amorphous phase in the crystal. However, in this work the β (T_g) and the α transition temperatures of the pristine PP did not change when the organoclay was used under any of the processing conditions.

Relationship between morphology and thermal properties

The crystallisation behaviour and the crystalline morphology of nanocomposites are strongly affected by the presence of layered silicates and their morphology[37]. The better the clay dispersion into the matrix is, the more crystal nuclei will be formed, and consequently, the higher will be the crystallisation temperature[38]. The organoclay increased slightly the crystallisation temperature (T_c) of the nanocomposites. Many authors consider this behaviour due to the nucleating effect of organoclay[1,14,19,39]. The PP/C20A samples increased 3 °C in the PP crystallisation temperature regardless of the profile and feed modes used, but did not change the $T_{c\ onset}$. The use of two different profiles and different feed modes did not affect the T_m and the X_c (Table 4). The neat PPP2 exhibited a lower crystallisation temperature than the neat PPP1. The larger shear of profile 2 accelerated the initial and the final degradation of the

Table 3. Mechanical and dynamic mechanical properties of PP/5%C20A nanocomposites and neat PP.

Samples	Young Modulus (MPa)	Storage Modulus at 23 °C (MPa)	Impact Strenght (J/m)	Yield Strength (MPa)	Yield Strain (%)
PP P1	1668 ± 35	1123	37 ± 3	30 ± 3	15 ± 0.5
PP P2	1697 ± 45	1118	45 ± 6	31 ± 1	15 ± 0.3
PP C20A P1	1917 ± 49	1206	43 ± 7	28 ± 1	17 ± 0.9
PP C20A P2	2349 ± 67	1551	65 ± 6	31 ± 0.8	18 ± 0.1
PP C20A P2SF	2131 ± 60	1526	52 ± 5	32 ± 0.4	18 ± 0.3

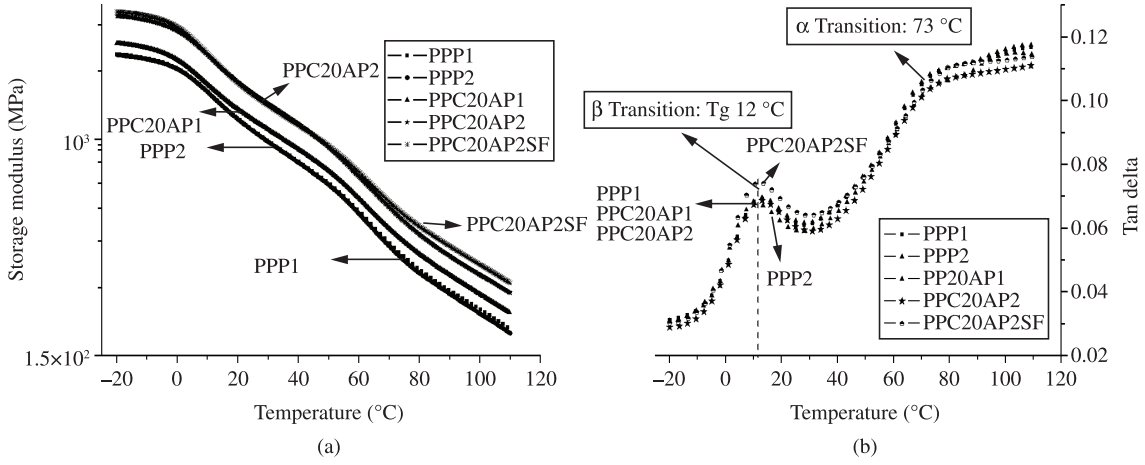

Figure 4. The storage modulus (a) and the tan δ peak: β transition and α transition (b) of the neat PP and PP/C-20A nanocomposites.

Table 4. DSC results for neat PP and PP/5%C20A nanocomposites.

Samples	T_m *(°C)	$T_{c\ (peak)}$ *(°C)	$T_{c\ (onset)}$ (°C)	X_c**(%)
Neat PP P1	164	116	120	46
Neat PP P2	164	114	120	44
PP C20A P1	165	119	121	38
PP C20A P2	164	116	120	32
PP C20A P2SF	165	117	120	42

*standard deviation ± 1 °C. **standard deviation ± 10%

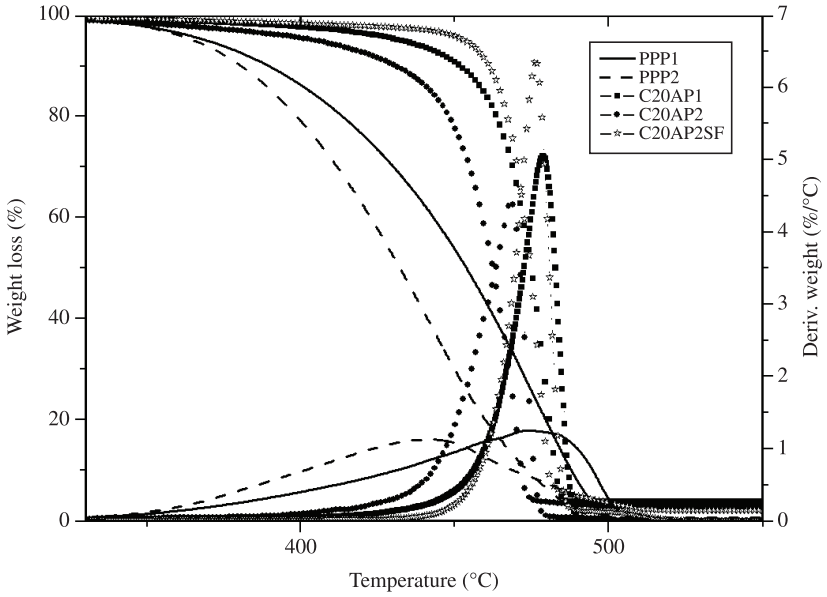

Figure 5. TGA and DTG curves of the neat PP and the PP/C20A nanocomposites.

neat PP probably because it promoted an increase in the polymeric mass temperature during the melt process, which quickly consumed a large amount of the antioxidant (Figure 5). The addition of clay into the PP matrix improved its thermal stability independent of the profile or the feed type used. All the PP nanocomposites exhibited an increased initial decomposition temperature (T_{onset}) compared to the neat PP at approximately 60 °C because MMT migrated to the surface and formed a protective barrier that impeded the release of decomposition gases, decreasing the degradation temperature of the PP matrix[40]. The PPC20AP2SF presented an initial and a final degradation higher than the other samples probably because of the presence of a mixture of elongated and elliptical structures and the smaller residence time in profile 2.

Conclusions

This work has shown the importance of screw profile design in the structure and properties of nanocomposites. The different shear intensities used to prepare the PP/C20A nanocomposites led to differences in the morphology, the mechanical and the thermal properties. The PPC20AP1 presented elliptical agglomerated structures with platelets that were more compacted, whereas the PPC20AP2 presented an elongated form with platelets that were more separated with a better clay distribution into the PP matrix. When the side feeder mode was used, a mix of elliptical and elongated structures with some individual clay sheets was observed. Profile 2 was more efficient at separating the C20A platelets into the PP matrix. The gain in the tensile modulus and the impact strength was more evident when elongated structures with better separated platelets were present. The presence of clay using two different profiles and two different feed modes did not influence the T_m and the X_c, but it did increase the T_c. The addition of clay into the PP matrix improved its thermal stability independent of the profile or the feeding type used.

Acknowledgements

The authors thank Braskem Petrochemical S.A., CNPq, FAPERGS and Finep for financial and technical support.

References

1. Ciardelli, F.; Coiai, S.; Passaglia, E.; Pucci, A. & Ruggeri, G. - Polym. Int., **57**, p.805 (2008). http://dx.doi.org/10.1002/pi.2415
2. Furlan, L. G.; Ferreira, C. I.; Dal Castel, C.; Santos, K. S.; Mello, A. C. E.; Liberman, S. A.; Oviedo, M. A. S. & Mauler, R. S. - Mater. Sci. Eng.: A, **528**, p.6715 (2011). http://dx.doi.org/10.1016/j.msea.2011.05.044
3. Wang, Y.; Chen, F-B. & Wu, K-C. - J. Appli. Polym. Sci., **93**, p.100 (2004).
4. Chavarria, F.; Shah, R. K.; Hunter, D. L. & Paul, D. R. - Polym. Eng. Sci., **47**, p.1847 (2007). http://dx.doi.org/10.1002/pen.20894
5. Diagne, M.; Guèye, M.; Vidal, L. & Tidjani, A. - Polym. Degrad. Stabil., **89**, p.418 (2005). http://dx.doi.org/10.1016/j.polymdegradstab.2005.01.032
6. Hasegawa, N.; Okamoto, H.; Kato, M. & Usuki, A. - J. Appli. Polym. Sci., **78**, p.1918 (2000).
7. Paiva, L. B.; Morales, A. R. & Guimarães, T. R. - Polímeros, **16**, p.136 (2006).
8. Silva, R. P; Mauler, R. S.; Oliveira, R. V. B. & Salles, C. A. - Polímeros, **20**, p.46 (2010). http://dx.doi.org/10.1590/S0104-14282010005000012

9. Zacharuk, M.; Becker, D.; Coelho, L. A. F. & Pezzin, S. H. - Polímeros, **21**, p.73 (2011). http://dx.doi.org/10.1590/S0104-14282011005000009
10. Rodolfo Junior, A. & Mei, L. H. I. - Polímeros, **19**, p.1 (2009). http://dx.doi.org/10.1590/S0104-14282009000100006
11. Zhu, L. & Xanthos, M. - J. Appli. Polym. Sci., **93**, p.1891 (2004).
12. Oliveira, M. F. L.; Oliveira, M. G. & Leite, M. C. A. M. - Polímeros, **21**, p.78 (2011) http://dx.doi.org/10.1590/S0104-14282011005000015
13. Farias, L. I.; Loureiro, M. O.; Raposo, C. M. O.; Canedo, L. E.; Carvalho, L. H. & Silva, S. M. L. - Polímeros, **21**, p.195 (2011).
14. Santos, K. S.; Liberman, S. A.; Oviedo, M. A. S. & Mauler, R. S. - J. Polym. Sci. : Part B: Poly. Phys., **46**, p.2519 (2008).
15. Wang, Z. M.; Nakajimia, H.; Manias E. & Chung, T. C. - Macromolecules, **36**, p.8919 (2003). http://dx.doi.org/10.1021/ma0352911
16. Sinha Ray S. & Okamoto, M. - Prog. Polym. Sci., **28**, p.1539 (2003). http://dx.doi.org/10.1016/j.progpolymsci.2003.08.002
17. Paul, D. R. & Robeson, L. M. - Polymer, **49**, p.3187 (2008). http://dx.doi.org/10.1016/j.polymer.2008.04.017
18. Pavlidou, S. & Papaspyrides, C. D. - Prog. Polym. Sci., **33**, p.1119 (2008). http://dx.doi.org/10.1016/j.progpolymsci.2008.07.008
19. Santos, K. S.; Liberman, S. A.; Oviedo, M. A. S. & Mauler, R. S. - Composites: Part A, **40**, p.1199 (2009). http://dx.doi.org/10.1016/j.compositesa.2009.05.009
20. dal Castel, C.; Liberman, S. A.; Oviedo, M. A. S.; Oliveira, R. V. B. & Mauler, R. S. - J. Appl. Polym. Sci., **121**, p.389 (2011). http://dx.doi.org/10.1002/app.33605
21. Santos, K. S.; dal Castel, C.; Liberman, S. A.; Oviedo, M. A. S. & Mauler, R. S. - J. Appl. Polym. Sci., **119**, p.1567 (2011). http://dx.doi.org/10.1002/app.32828
22. Dennis, H. R.; Hunter, D. L.; Chang, D.; Kim, S.; White, J. L. & Cho, J. W. - Polymer, **42**, p.9513 (2001). http://dx.doi.org/10.1016/S0032-3861(01)00473-6
23. Lertwimolnun, W. & Vergnes, B. - Polymer, **46**, p.3462 (2005). http://dx.doi.org/10.1016/j.polymer.2005.02.018
24. Santos, K. S.; Bischoff, E.; Liberman, S. A.; Oviedo, M. A. S. & Mauler, R. S. Ultrason. Sonochem., **18**, p.997 (2011). PMid:21486705. http://dx.doi.org/10.1016/j.ultsonch.2011.03.011
25. Gianelli, W.; Ferrara, G.; Camino, G.; Pellegatti, G.; Rosenthal, J. & Trombini, R. C. - Polymer, **46**, p.7037 (2005). http://dx.doi.org/10.1016/j.polymer.2005.05.149
26. Kohlgrüber, K. & Rudolf, R. - "Co-rotating twin-screw extruders: fundamentals, technology, and applications", Hanser Gardner, Carl Hanser publishers (ed), p.59-75, Munich (2008).
27. Hussain, F.; Hojjati, M.; Okamoto, M. & Gorga, R. - J. Comp. Mater., **40**, p.17 (2006). http://dx.doi.org/10.1177/0021998306067321
28. Esteves, A. C. C.; Timmons A. B. & Trindade, T. - Quím. Nova, **27**, p.798 (2004). http://dx.doi.org/10.1590/S0100-40422004000500020
29. Amash, A. & Zugenmaier, P. - J. Appli. Polym. Sci., **63**, p.1143 (1997).
30. Modesti, M.; Lorenzetti, D. & Besco, B. S. - Polymer, **46**, p.10237 (2005). http://dx.doi.org/10.1016/j.polymer.2005.08.035
31. Dong, Y. & Bhattacharyya, D. - Composites Part A, **39**, p.1177 (2008). http://dx.doi.org/10.1016/j.compositesa.2008.03.006
32. Sun, L.; Gibson, R. F.; Gordaninejad, F. & Suhr, J. - Compos. Sci. Technol., **69**, p.2392 (2009). http://dx.doi.org/10.1016/j.compscitech.2009.06.020
33. Ha, S. R.; Rhee, K. Y.; Kim, H. C. & Kim, J. T. – Colloi. Surf. A: Physicochem. Eng. Aspects., **313**, p.112 (2008). http://dx.doi.org/10.1016/j.colsurfa.2007.04.082
34. Wang, K.; Liang, S.; Deng, J.; Yang, H.; Zhang, L.; Fu, Q.; Dong, X.; Wang, D. & Han, C. C. - Polymer, **47**, p.7131 (2006). http://dx.doi.org/10.1016/j.polymer.2006.07.067
35. Tanniru, M.; Yuan, Q. & Misra, R. D. K. - Polymer, **47**, p.2133 (2006). http://dx.doi.org/10.1016/j.polymer.2006.01.063
36. Galgali, G.; Agarwal, S. & Lele, A. - Polymer, **45**, p.6059 (2004). http://dx.doi.org/10.1016/j.polymer.2004.06.027
37. Perrin-Sarazin, F.; Ton-That, M.; Bureau, M. & Denault, J. - Polymer, **46**, p.11624 (2005). http://dx.doi.org/10.1016/j.polymer.2005.09.076
38. Sharm, S. K. & Nayak, S. K. - Polym. Degrad. Stabil., **94**, p.132 (2009).
39. Dong, Y. & Bhattacharyy, D. – Mater. Sci. Eng. A, **527**, p.1617 (2010). http://dx.doi.org/10.1016/j.msea.2009.10.043
40. Tang, Y. & Lewin, M. - Polym. Degrad. Stabil., **92**, p.53 (2007). http://dx.doi.org/10.1016/j.polymdegradstab.2006.09.013

Received: 13/03/12
Revised: 03/07/12
Accepted: 20/07/12